ORIGINAL RESEARCH ARTICLE

The Depositional Record ⟨Open Access⟩
A journal of the International Association of Sedimentologists

IAS · **WILEY**

Microfacies analysis of the Palaeocene Lockhart limestone on the eastern margin of the Upper Indus Basin (Pakistan): Implications for the depositional environment and reservoir characteristics

Ahmer Bilal[1] ⓘ | Renchao Yang[1,2] | Hammad Tariq Janjuhah[3] ⓘ | Muhammad Saleem Mughal[4] | Yang Li[1] | George Kontakiotis[5] ⓘ | Nils Lenhardt[6]

[1]Shandong University of Science and Technology, Qingdao, China

[2]Shandong Provincial Key Laboratory of Depositional Mineralization & Sedimentary Minerals, Shandong University of Science and Technology, Qingdao, China

[3]Department of Geology, Shaheed Benazir Bhutto University Sheringal, Upper Dir, Khyber Pakhtunkhwa, Pakistan

[4]Institute of Geology, University of Azad Jammu and Kashmir, Muzaffarabad, Pakistan

[5]Department of Historical Geology-Paleontology, Faculty of Geology and Geoenvironment, School of Earth Sciences, National and Kapodistrian University of Athens, Athens, Greece

[6]Department of Geology, University of Pretoria, Pretoria, South Africa

Correspondence
Renchao Yang, Shandong University of Science and Technology, 266590, Qingdao, China.
Email: yang100808@126.com

Hammad Tariq Janjuhah, Department of Geology, Shaheed Benazir Bhutto University Sheringal, Upper Dir, Khyber Pakhtunkhwa 18000, Pakistan.
Email: hammad@sbbu.edu.pk

Abstract

A detailed sedimentological analysis of the Palaeocene Lockhart Limestone has been conducted to evaluate the depositional environment, diagenetic processes and hydrocarbon potential of the eastern margin of the Upper Indus Basin. From bottom to top, there are three microfacies recorded. The lower microfacies, composed of fine-grained micrite and some diagenetic dolomite, reflect the low energy and calm palaeo-current in the shallower section (1–2 m) of the inner shelf close to shore. The middle microfacies contain algae that suggest 5–15 m of water depth, especially along the inner-middle shelf, but fractured and mixed bioclasts in micrite material indicate calm to moderately active water close to the wave base. Progressing from the lower microfacies to the middle microfacies, a gradual shift from orthochem to allochem components is observed. The top microfacies is dominated by massive benthic microfossils, indicating moderate energy-water conditions with normal salinity. However, the presence of limestone intraclasts surrounded by microspar, miliolids and nummulites at the top indicates a high-energy environment with increasing salinity and water depths from 20 to 130 m. These findings show that the Lockhart Limestone was deposited in a shallow shelf environment, spanning the inner-mid shelf. Diagenetic processes observed include micritisation, cementation, dissolution, replacement, physical and chemical compaction, and fracture filling

by calcite cement. The Lockhart Limestone represents a deepening upward sequence deposited below the shelf margin system tract and highstand systems tract in a regressive environment that could reflect good reservoir characteristics, has the potential to serve as an excellent hydrocarbon reservoir rock, and could be a primary target for future hydrocarbon exploration.

1 | INTRODUCTION

The Indus Basin (IB), a major sedimentary basin of Pakistan, is approximately 873,000 km² in size (Figure 1A) (Wandrey et al., 2004). Tectonically, the basin is bounded from the north-eastern and western sides by the Main Boundary Thrust (MBT) and the Chaman Transform Fault (CTF) respectively (Ali et al., 2021; Awais et al., 2019). The IB has been further subdivided into the Upper Indus Basin (UIB), Central Indus Basin (CIB) and Southern Indus Basin (SIB), and it is a major source of hydrocarbons in the area (Figure 1B) (Ehsan et al., 2021; Shah, 2009). Highs separate the UIB and CIB from the south and the Kurram Thrust towards the west, while MBT delineates the northern and eastern boundaries of the UIB (Badshah et al., 2000). The UIB consists of sedimentary rocks ranging in age from the Precambrian to the recent. However, the research region is located on the UIB's eastern boundary and is composed of sedimentary, metamorphic and igneous rock types (Figure 2; Table 1).

In recent years, emphasis has been placed on the stratigraphy, structure, geophysics and palaeontology of the UIB's nearby eastern margin (Afzal et al., 2009; Akhtar et al., 2019; Khan et al., 2018; Munir et al., 2006). However, a few researchers have conducted reconnaissance studies focussing on particular geological aspects such as tectonic framework and mineralogy (Figure 2A,B) (Ashraf & Chaudhary, 1984; Nawaz & Mn, 1980) and the geological characteristics of the area are difficult to understand as this region is part of a fold and thrust belt.

The meta-sediments of Dogra Slates (Neo-Proterozoic Era) are unconformably overlain by the Cambrian Kailar Formation (Table 1). The Kailar Formation consists mostly of dolomites and dolomitic limestone (Ashraf & Chaudhary, 1984). The upper contact of the Kailar Formation with the Permian Panjal Formation is also unconformable (Ashraf & Chaudhary, 1984). A large unconformity separates the Panjal Formation from the Palaeocene-Eocene rocks (Bilal & Khan, 2017). The upper contact between the Middle Eocene to Early Oligocene Kuldana Formation and the Early Miocene Murree Formation is also unconformable.

At the top of the succession, the Murree Formation and the Recent Alluvium are separated by an angular unconformity (Table 1) (Mughal et al., 2018).

Due to its type location near Fort Lockhart in the Samana Range, the nodular limestone of Palaeocene age is referred to as the Lockhart Limestone (Davies, 1930; Shah, 2009). The Lockhart Limestone is a hydrocarbon reservoir in the UIB (Awais et al., 2019; Shakir et al., 2019). Most of the nodular limestone deposits on the shallow shelf, particularly in the inner-mid-shelf, are highly significant because they have historically served as suitable reservoirs across Europe, the Middle East and Asia (Awais et al., 2019; Reza, 2014; Yang et al., 2017). In addition to being exposed across the UIB, it is also exposed at the eastern margin of the UIB although detailed investigation of the Lockhart Limestone in this area was beyond the scope of this study.

The lack of information regarding the Lockhart Limestone, particularly with regards to age, diagenesis and depositional environment, is a significant issue in the research region that has to be addressed. This research will be used to cross-correlate the Lockhart Limestone regionally and throughout the UIB and to comprehend the geological and sedimentological characteristics of the Lockhart Limestone in this region (Figure 2B). Additionally, the depositional and diagenetic features of the Lockhart Limestone were addressed to determine its reservoir characteristics. These were derived through in-depth analyses of litho-biofacies used to reconstruct depositional settings and identify relevant diagenetic processes for the petroleum industry.

2 | METHODS AND MATERIALS

The texture and composition of carbonate rocks can be used to understand their depositional setting (Janjuhah et al., 2017a, 2021). For the purpose of petrographic microfacies identification, 40 limestone samples from the Haveli Section (LC1 to LC40) were collected at equal intervals of 3.7 m (Figure 3). The Haveli Section is located on the eastern margin of UIB and is bordered by latitudes of 33 55′0″ to 33 58′0″ North and longitudes of 74 8′0″ to
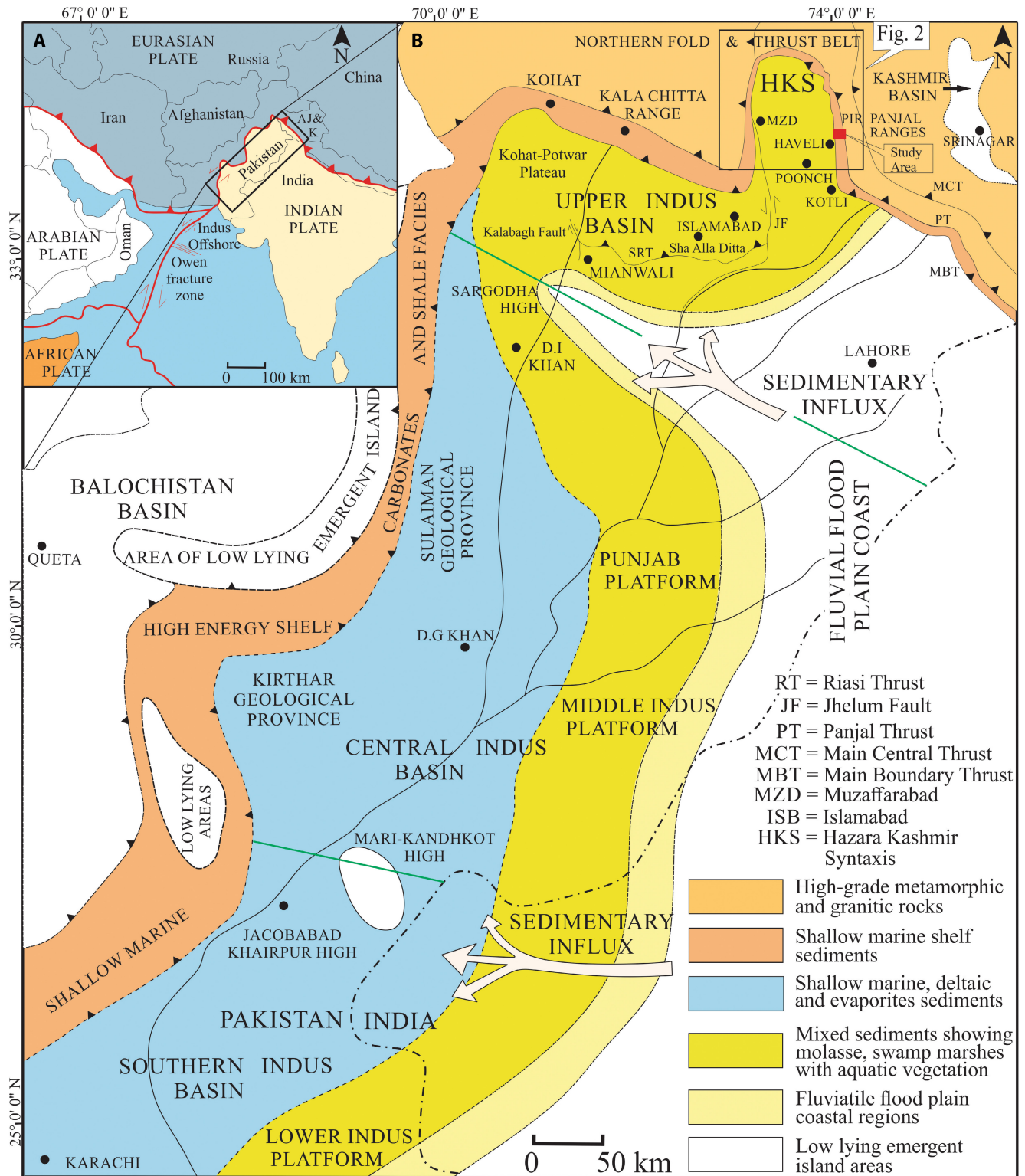
FIGURE 1 (A) Pakistan regional map. (B) A general geological map depicting the locations of the Indus Basin and its eastern margin, modified after Shah (2009).

74 11′0″ East (Figure 2B). The thickness of the formation was determined using the Jacob's Staff method, which led to the preparation of the section's litholog. Field images were taken using a digital camera (Figure 3A through E). Thin section preparation was carried out at the Shandong University of Science and Technology (China). A polarising microscope, the LEICA-DM 750P with a connected LEICA-EC3 camera (Leica Microsystems Ltd.), was then used in the laboratory to identify and categorise the fossil content and to determine the mineralogical composition.
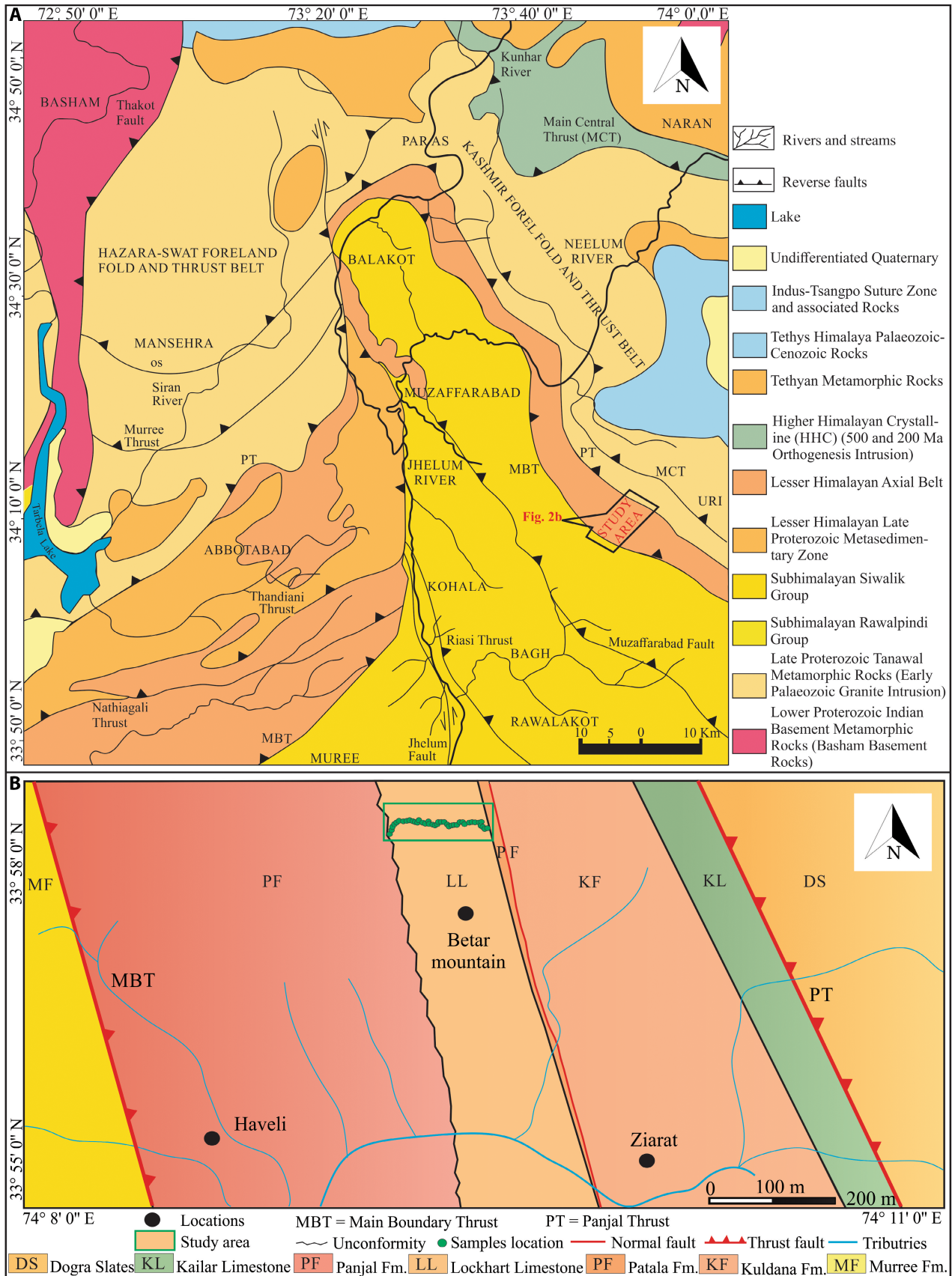
FIGURE 2 (A) Geological map of the Hazara Kashmir Syntaxis (HKS) and UIB's eastern margin, based on Nawaz and Mn (1980). (B) A geological map of the study area.

TABLE 1 Stratigraphy of different areas in the IB (Shah, 2009).

| System/Period	Series/Epoch/Stage		Azad Jammu & Kashmir	Axial Belt	Study Area	Upper Indus Basin	Middle Indus Basin	Lower Indus Basin
Quaternary	Holocene		Alluvium Mirpur Conglomerate	Mirpur Conglomerate Bostan Fm. Haro Conglomerate	Alluvium	Alluvium Lei Conglomerate	Alluvium Lei Conglomerate	Alluvium Lei Conglomerate
	Pleistocene							
Neogene	Pliocene		Soan Fm. Dhoke Pathan Fm.	Soan Fm. Dhoke Pathan Fm.		Soan Fm. Dhoke Pathan Fm.	Soan Fm. Dhoke Pathan Fm.	Soan Fm. Dhoke Pathan Fm.
	Miocene		Nagri Fm. Chingi Fm. Kamlial Fm. Murree Fm.	Nagri Fm. Hinglaj Fm. Gaj Fm.	Murree Fm.	Nagri Fm. Chingi Fm. Kamlial Fm. Murree Fm.	Nagri Fm. Chingi Fm.	Nagri Fm. Chingi Fm. Gaj Fm.
Palaeogene	Oligocene			Nari Fm.				Nari Fm.
	Eocene		Kuldana Fm. Chorgali Fm. Margala Hill Limestone	Kirthar Fm. Ghazij Fm. Nisai Fm. Dungan Fm.	Kuldana Fm.	Kuldana Fm. Chorgali Fm. Sakesar Limestone Nammal Fm. Margala Hill Limestone	Kirthar Fm. Ghazij Group Laki/Sui Main Limestone	Kirthar Fm. Ghazij Group Laki/Sui Main Limestone
	Palaeocene	Thanetian	Patala Fm. Lockhart Limestone	Lakhra Fm. Bara Fm. Khadro Fm. Rakhshani Fm.	Patala Fm. Lockhart Limestone	Patala Fm. Lockhart Limestone.	Ranikot Fm.	Ranikot Fm.
		Selandian Danian	Hangu Fm.			Hangu Fm.		
Cretaceous	Upper			Pab Sandstone Moro Fm.		Kawagarh Fm.	Pab Sandstone Fort Munro Fm. Mughalkot Fm. Par Limestone Goru Fm. Sember Fm.	Pab Sandstone Fort Munro Fm. Mughalkot Fm. Par Limestone Goru Fm. Sember Fm.
	Lower			Bela Volcanic Group		Lumshiwal Fm. Chichali Fm.		
Jurassic	Upper					Samanasuk Fm. Shinwari Fm. Datta Fm.	Chiltan Fm.	Chiltan Fm. Shirinab Fm.
	Lower							
Triassic	Upper					Kingriali Fm. Tredian Fm. Mianwali Fm.	Wulgai Fm.	Wulgai Fm.
	Middle							
	Lower							
Permian	Lopingian			Attock Fm.	Panjal Fm.	Chidru Fm. Wargal Limestone Amb Fm. Sardhai Fm. Warcha Sandstone Dandot Fm. Tobra Fm.	Not exposed or drilled	Not exposed or drilled
	Cisuralian			Khyber Limestone				
Carboniferous				Khyber Carbonates				
Devonian	Upper			Misri Banda Quartzite				
	Lower			Nowshera Fm.				
Silurian				Kandar Phyllite				
Ordovician				Attock Fm.				
Cambrian	Furongian Miaolingian Series 2		Abbottabad Fm.	Hazira Fm. Abbottabad Fm. Tanawul Fm.	Kailar Fm.	Baghanwala Fm. Jutana Fm. Kussak Fm. Khewra sandstone		
Precambrian	Proterozoic		Hazara Fm. / Dogra Slates	Hazara Fm. / Dogra Slates	Hazara Fm. / Dogra Slates	Salt range Fm. Crystalline Bascement		
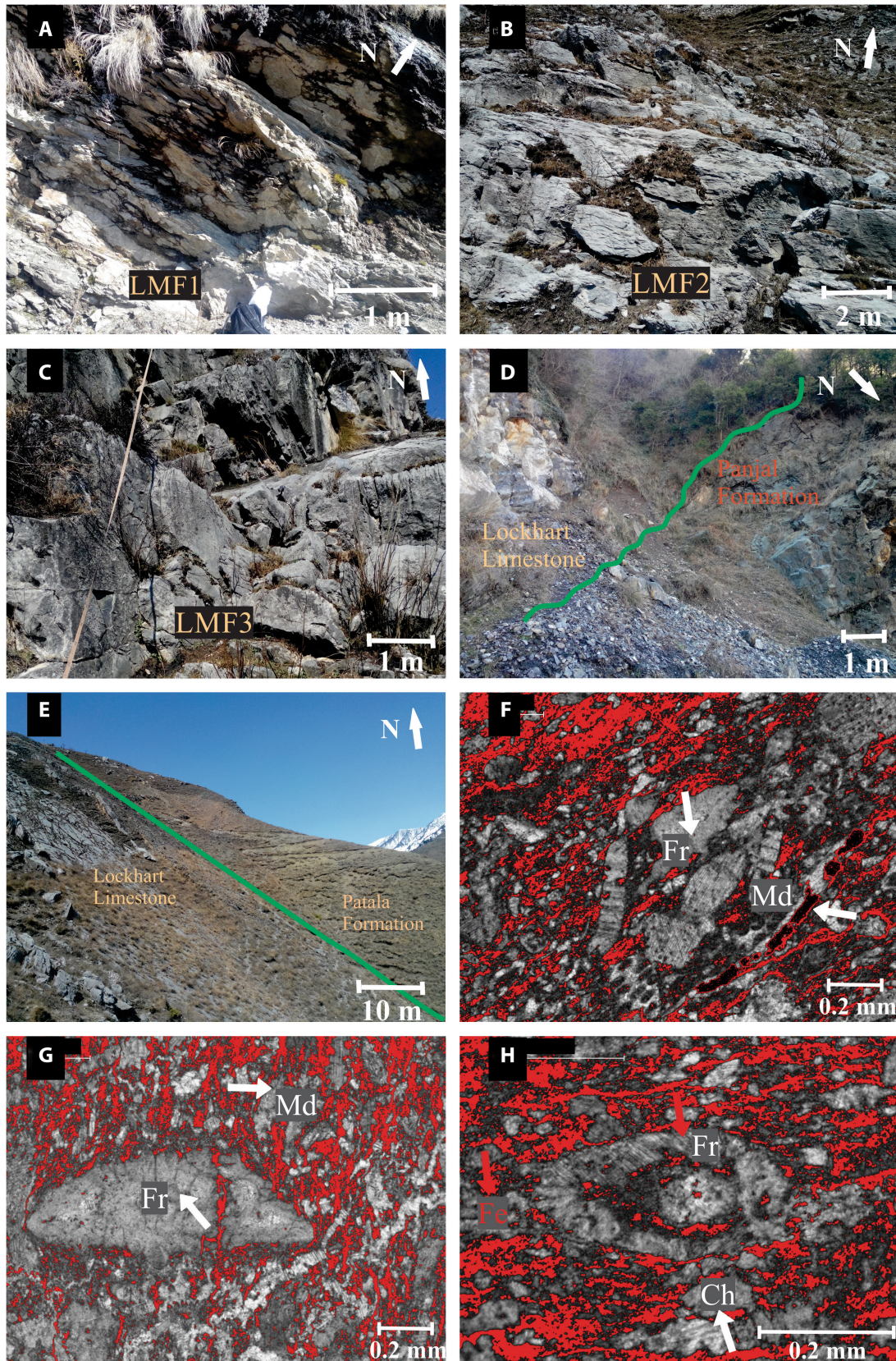
FIGURE 3   (A through D) Base microfacies with unconformable lower contact of Lockhart Limestone with Panjal Formation; (E) Upper contact of Lockhart Limestone with Patala Formation. Image threshold enhancement technique in ImageJ software revealed pore spaces and their types in three microfacies of the Lockhart Limestone. (F and G) 16% porosity with fracture (Fr) and mouldic (Md) types, respectively; (H) 21% porosity with fracture, fenestral (Fe) and channel (Ch) types in Lockhart Limestone.

The petrographic and field data were interpreted according to Dunham's (1962) classification scheme for establishing microfacies by comparing it with those of Flügel and Munnecke (2010) and Wilson (1974). Microfossils in the same thin sections were identified to evaluate their specific depositional realm and for stratigraphic purposes in a relative geochronological study. The bibliography of Flügel and Munnecke (2010) was used to determine foraminiferal microfossils. The Imagej software was then used to compute the effective porosity using the image threshold approach (Figure 3F,G,H).

3 | RESULTS

During the Palaeocene, a broad carbonate shelf covered the northern parts of the IB. The resultant carbonate rocks of the Lockhart Limestone are variably classified as the source, reservoir and cap rocks within the basin, giving them a crucial role not just in basin analysis, but also in hydrocarbon exploration within the basin. The following litho-biofacies are identified by field and petrographic investigations of the Lockhart Limestone along the eastern margin of the UIB.

3.1 | Integrated carbonate lithofacies and biofacies

In general, the limestone is hard and exhibits a light to dark grey colour within the study area (Figure 3A through E). A diversity of fossils, including algae and foraminifers (Figure 3F,G,H), were detected throughout the section. Fossils are only present in the middle (above 40–84 m, towards the middle of the section) and at the top (above 121–151 m, towards the middle of the section) of the sequence. After an erosional contact, the shale of the Patala Formation covers the limestone rocks (Figure 4).
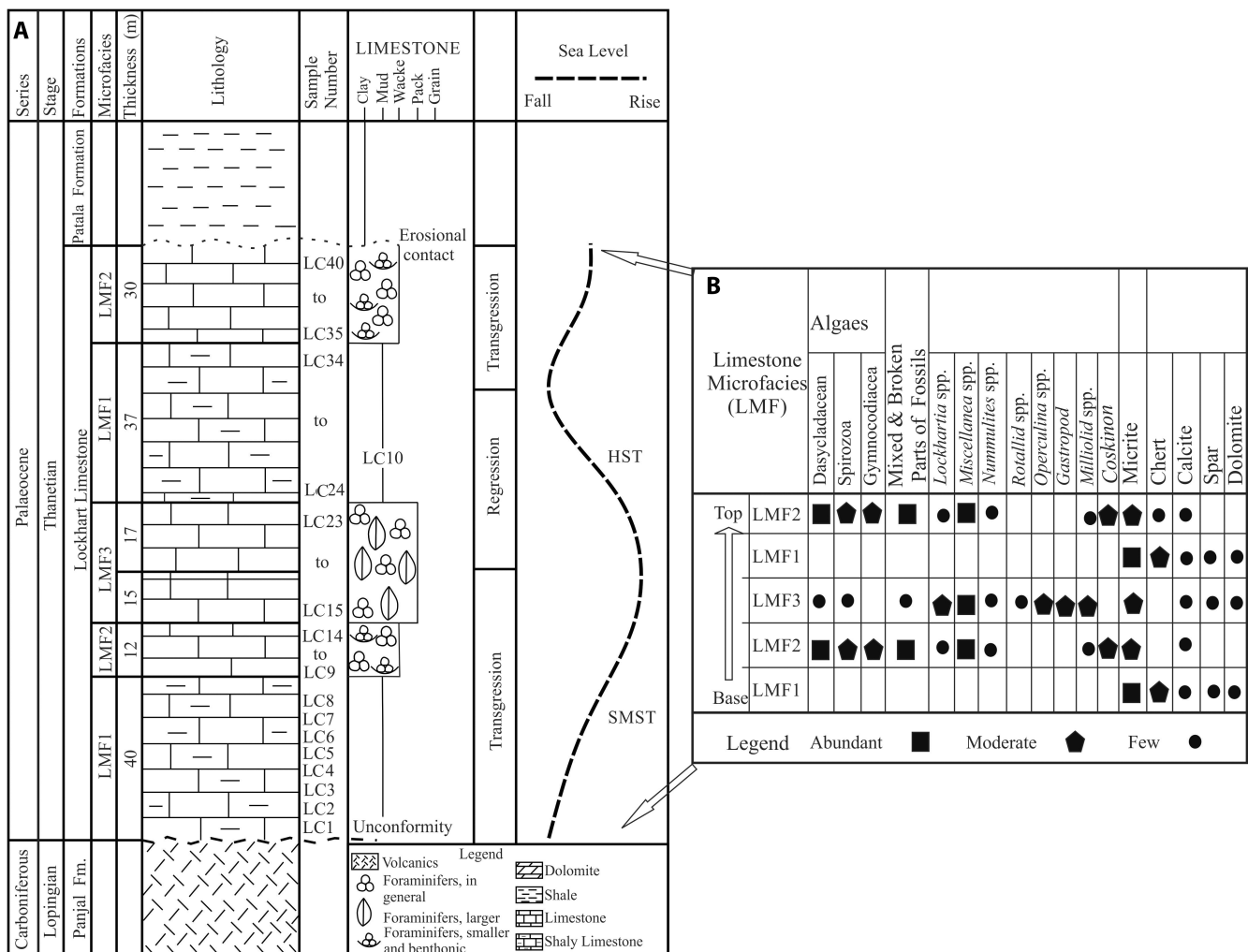

FIGURE 4 (A) Lithostratigraphic column of the Lockhart Limestone. See Figure 2B for location. HST, Highstand systems tract; SMST, shelf margin systems tract. (B) Occurrence and abundance of fossils in the Lockhart Limestone.

3.2 | Pore types

Most of the pores in the studied samples are either mouldic or intraparticle (Figure 3F,G,H). Choquette and Pray (1970) classify pores into intraparticle, mouldic, vuggy, fracture and interparticle pores, features observable in Figure 5A through G.

3.3 | Quantitative analysis

An analysis of all Lockhart Limestone thin sections revealed that the rock is composed of fine to medium-sized grains that are free of mud. The majority of the rock is limestone (90%) and dolomite (10%). (Figure 5A). Packstone was identified in 35% of thin sections from all rock samples (lower, middle and upper sections), whereas the remaining 65% were classified as wackestone, mudstone or grainstone (Figure 5B). A total of 40% of the Lockhart Limestone consists of grains, while the other 54% is composed of matrix and cement. The remaining 6% can be attributed to porosity (Figure 5C). In a qualitative study of the visible porosity, five distinct pore types were identified (Figure 5D), vuggy (35%), intraparticle (25%), interparticle (20%), fracture (10%) and mouldic (10%) (Figure 5D).

3.4 | Microfacies analysis

The Lockhart Limestone from the eastern margin of UIB exhibits three lithofacies from base to top (Figure 3A,B,C). The lower part consists of dark grey-coloured, thinly bedded limestone (Figure 6A,B). A light grey-coloured, medium-bedded, fused nodular and fossiliferous limestone was identified above this (Figure 3B). The third identified lithofacies at the top of the sequence is a grey-coloured, thick-bedded and highly fossiliferous limestone (Figure 3C). Petrographic analysis shows that the Lockhart Limestone comprises spar, micrite and allochem particles (Table 2). By integrating lithofacies with petrographic results in accordance with Dunham's (1962) classification scheme, the formation was categorised into three major microfacies types: (1) mudstone-wackestone carbonate microfacies (LMF1); (2) algal-foraminiferal mixed bioclastic mudstone–packstone microfacies (LMF2); and (3) benthic foraminiferal wacke–packstone microfacies (LMF3).

Among the observed bioclasts are: Dascycladacean green algae, Spirozoa algae, *Assilina* spp, *Operculina* spp, *Lockhartia* spp, *Miscellanea* spp, *Echinoid* spine and *Quinqueloculina* spp (Figure 4). All fossils are recrystallised.
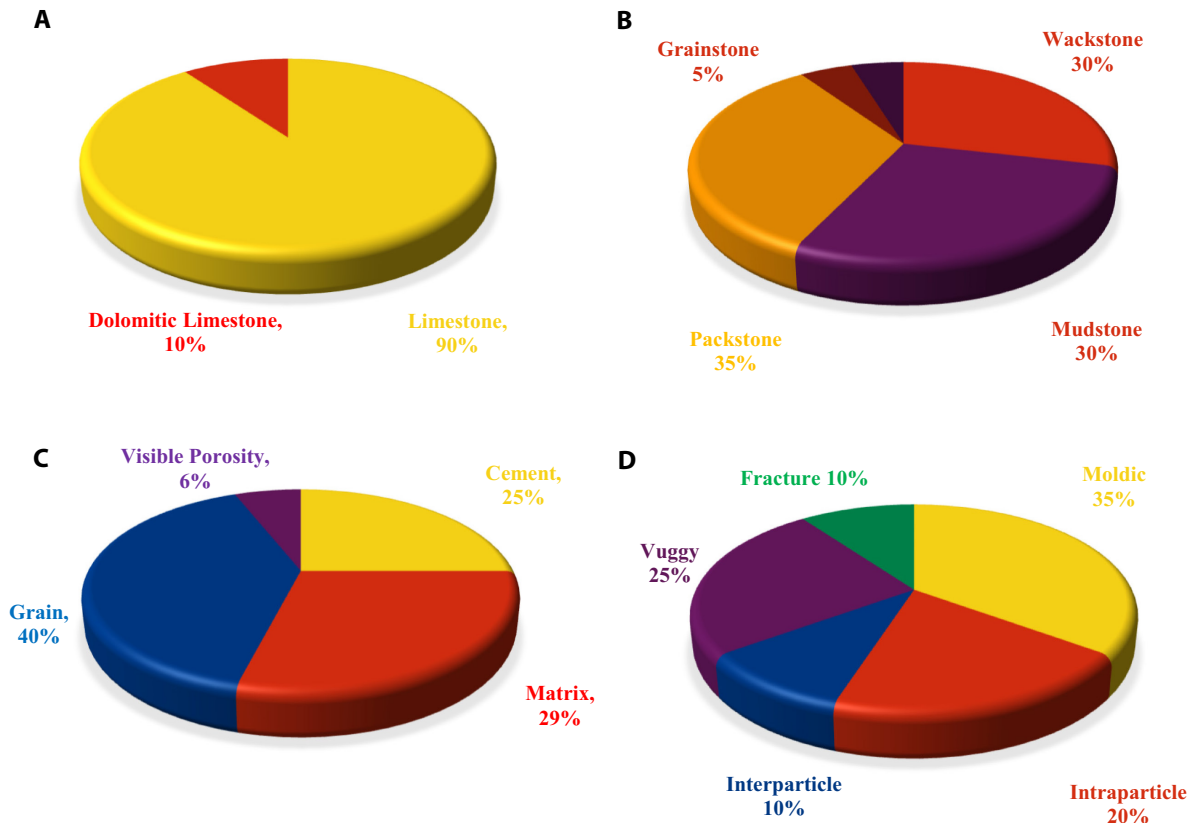

FIGURE 5 Graphics depicting: (A) the quantitative distribution of microfacies, (B) the rock components and textures, (C) the quantitative distribution of grains, matrix and cement and (D) the various pore types in the studied samples.
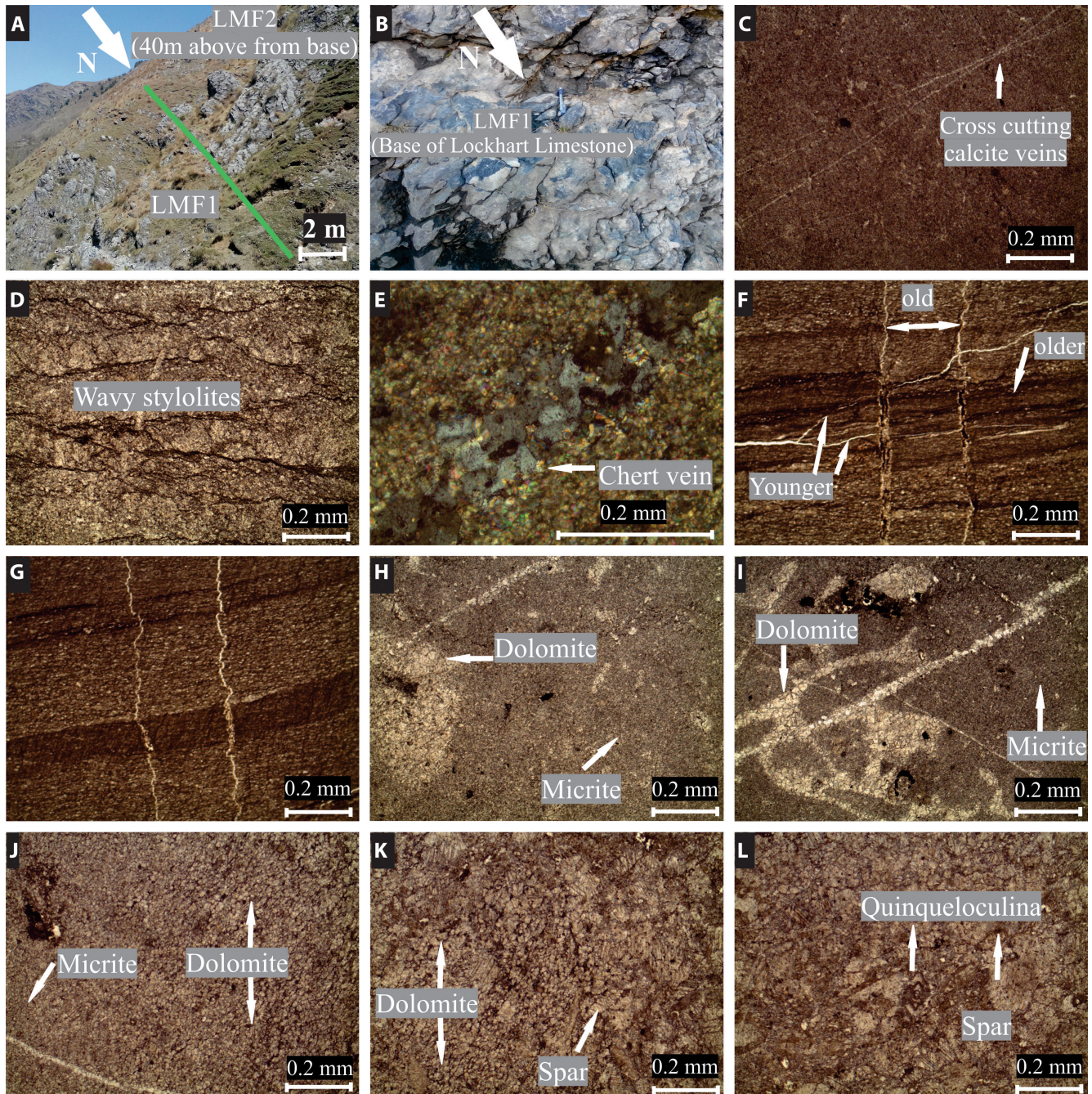
FIGURE 6 Photomicrographs and outcrop images of the mudstone-wackestone carbonate microfacies (LMF1): (A) Outcrop contact of LMF1 and LMF2 near the base; (B) Nodular limestone near the base; (C) Cross-cutting calcite veins; (D and E) Wavy lamination and chert in LMF1 respectively; (F and G) Cross-cutting calcite veins in thinly laminated sub-microfacies; (H and I) Dolomite crystals in micrite; (J, K, L) a gradual change from micrite dolomite which further altered into the spar.

3.4.1 | Mudstone-wackestone carbonate microfacies (LMF1)

Description: This microfacies is characterised by 1–5 cm of thickly bedded limestone, which is dark grey to brownish in colour and moderately fractured (Figures 3A and 6A,B). The LMF1 occurs between 0 and 40 m above the base of the section and between 84 and 121 m in the upper part of the section (Figure 4A). Both the lower and upper contacts of the Lockhart Limestone are unconformable with the Panjal Formation and the Patala Formation, respectively (Figure 6A through E; Table 2).

Thin section analysis characterised the rock as mudstone and wackestone. Allochems (5%) and micrite matrix (90%) are the major constituents, with 5% of the grains consisting of chert, with sizes ranging from 0.02 to 0.3 mm (Table 2). Spar, calcite veins and stylolites are prominent

TABLE 2 Skeletal and non-skeletal components of the microfacies.

S. no	Spar (%)	Micrite (%)	Bioclasts (%)	C.M (%)	Pyrite (%)	Calcite (%)	Hematite (%)	Chert (%)	Dolomite (%)	Dunham classification
LC1	1	90	-	2	-	4	-	3	-	Mudstone - Wackestone
LC2	1	89	-	3	-	5	-	2	-	
LC3	4	81	-	1	-	10	1	-	3	
LC4	3	80	2	-	1	10	-	3	1	
LC5	-	85	3	-	-	8	1	3	-	
LC6	3	79	-	-	-	10	-	-	8	
LC7	2	81	4	-	1	3	-	2	7	
LC8	17	56	-	-	-	14	3	-	10	
LC9	-	22	70	3	-	5	-	-	-	Mudstone - Packstone
LC10	-	9	78	-	-	12	1	-	-	
LC11	1	24	70	1	1	3	-	-	-	
LC12	-	8	77	1	-	14	-	-	-	
LC13	-	20	75	-	-	12	1	-	-	
LC14	2	71	7	4	1	14	-	1	-	
LC15	-	30	35	3	-	32	-	-	-	Wacke- packstone
LC16	-	33	50	1	-	16	-	-	-	
LC17	2	20	60	-	1	16	1	-	-	
LC18	1	17	68	-	-	14	-	-	-	
LC19	10	12	73	2	1	2	-	-	-	
LC20	8	10	75	-	-	6	1	-	-	
LC21	-	30	37	2	-	31	-	-	-	
LC22	9	8	80	-	1	2	-	-	-	
LC23	10	10	75	3	-	2	-	-	-	
LC24	8	21	65	5	-	1	-	-	-	
LC25	-	93	-	-	2	1	-	4	-	Mudstone - Wackestone
LC26	4	85	4	2	-	2	1	2	-	
LC27	2	70	-	1	-	24	3	-	-	
LC28	3	87	2	3	1	1	-	3	-	
LC29	-	78	4	2	-	14	-	-	2	
LC30	5	72	-	-	-	16	-	4	3	
LC31	2	85	1	3	1	6	1	2	1	
LC32	-	74	1	-	-	15	-	-	10	
LC33	9	70	-	-	1	9	1	1	9	
LC34	10	48	10	-	-	20	-	-	12	
LC35	-	15	82	3	-	-	-	-	-	Mudstone - Packstone
LC36	2	22	76	-	-	-	-	-	-	
LC37	-	18	73	2	-	6	1	-	-	
LC38	-	20	68	1	1	10	-	-	-	
LC39	-	19	62	-	-	18	-	1	-	
LC40	1	89	3	3	1	3	-	-	-	

features of this microfacies and define the sub-microfacies shown in Figure 6C,D,E.

3.4.2 | Wavy laminated chert subfacies

This subfacies is distinguished by wavy lamination, whereas stylolites occur in the mudstone microfacies (Figure 6F).

Thin sections show internal deformation, tectonic veins and pressure dissolution features (Figure 6E).

3.4.3 | Thin laminated lateral subfacies

A thinly laminated subfacies (Figure 6G) with several calcite veins that cross-cut one another and lamina that

appear as lateral expansions along the undulating laminated chert sub-microfacies (Figure 6C,F).

3.4.4 | Micrite-dominated dolomite subfacies

Micrite (Figure 6H) has often been transformed into dolomite in this subfacies (Figure 6I). It is also characterised by a lack of organic material.

3.4.5 | Spar-dominated micrite to dolomite subfacies

There is a variation in which a complete sequence of alteration from micrite to dolomite (Figure 6J) is observed, which is thereafter converted into sparite (Figure 6K). The transformation of dolomite into sparry dolomite (Figure 6L) illustrates the de-dolomitisation process.
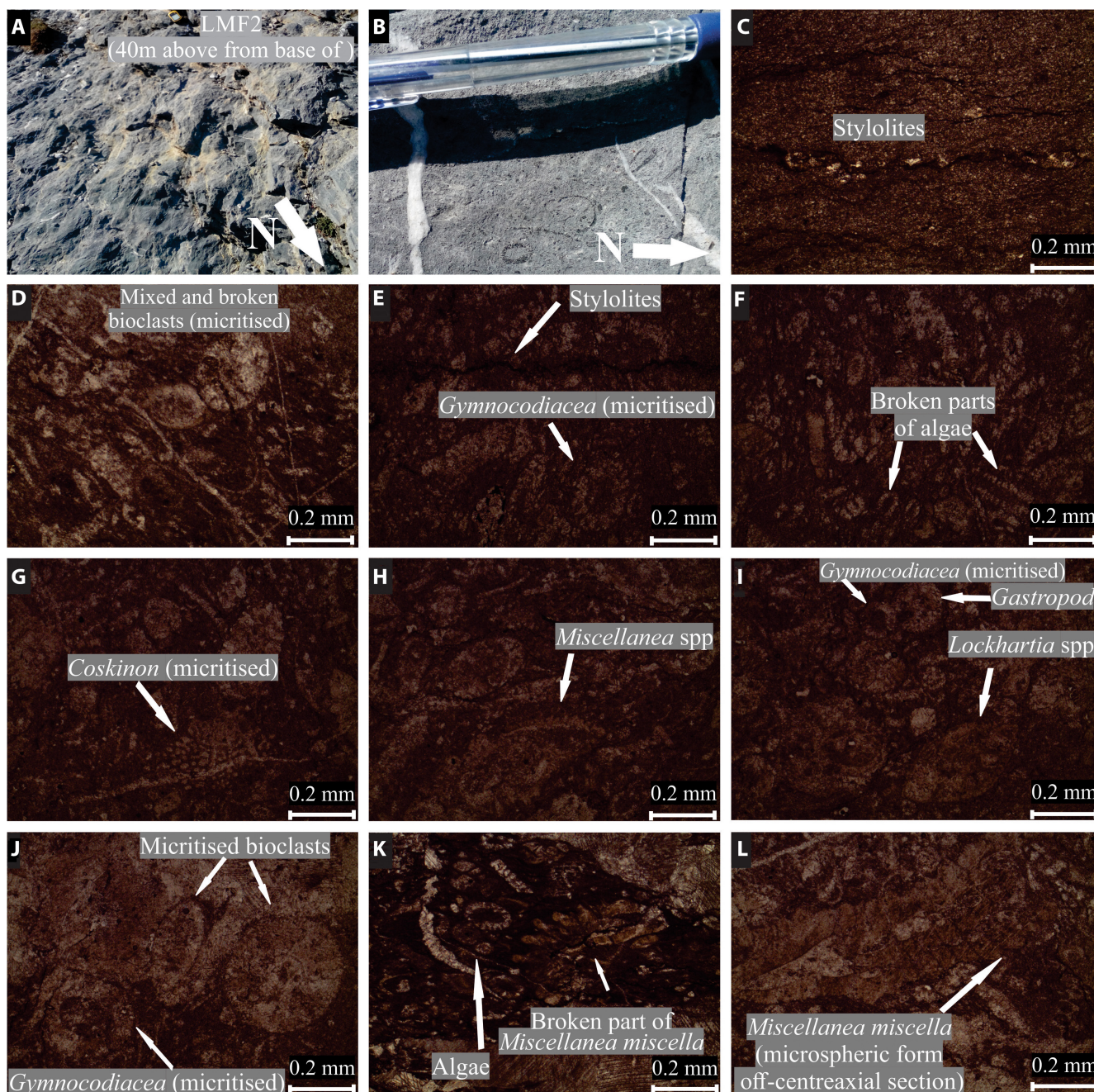

FIGURE 7 Outcrop images and photomicrographs of the algal-foraminiferal mixed bioclastic mudstone–packstone microfacies (LMF 2): (A) Fused nodules near the lower centre of the formation; (B) Bioclasts in an outcrop of LMF2; (C through L) Sedimentary features and bioclasts identified in LMF2.

3.4.6 | Algal-foraminiferal mixed bioclastic mudstone–packstone microfacies (LMF2)

Description: LMF2 is composed of medium-bedded light grey limestone (0.5–3 m) (Figure 7A,B). The upper and lower limits of the adjacent microfacies are defined gradationally. Thin section examination indicates a micrite concentration of up to 25%. The grain-clast content is 75% and 25% respectively. The clasts, which are mostly bioclasts, vary in size from 0.2 to 1 mm (Figure 7B). Dascycladacean algae, *Miscellanea* spp., *Gymnocodiacea*, *Coskinolina*, echinoid spines, and a variety of broken bioclasts are the most notable fossils within this facies (Figure 4).

3.4.7 | Fossiliferous and micrite matrix dominated subfacies

Micrite predominates after fossils in this subfacies, along with some stylolites (Figure 7C). Micrite usually contains mixed and broken fossil fragments (Figure 7D,E,F). This is a less abundant subfacies.

3.4.8 | Dascycladacea packstone subfacies

There are numerous bioclasts in this subfacies, and these bioclasts are commonly micritised (Figure 7G through L). There are also calcite veins (Figure 7G) and spar (Figure 7L).

3.4.9 | Benthic foraminiferal wacke–packstone microfacies (LMF3)

Description: This microfacies is characterised by 2–3 m of thick-bedded, nodular, light grey limestone with a significant fossil content (Figure 8A,B). This microfacies has a thickness interval of 32 m. Upper and lower boundaries are gradational with the adjacent microfacies. The matrix and (bio-) clast content of the samples may reach up to 20% and 75% respectively. A considerable number of fossils (Figure 8C through G) originate from algae and benthic foraminifera: *Lockhartia* spp. (Figure 8C), *Operculina* spp. (Figure 8D), *Rotallid* spp. (Figure 8H), *Miscellanea* spp. (Figure 8I,J), *Assilina spinose*, *Quinqueloculina* and additional gastropods (Figure 8B,E) and broken bioclasts (Figure 8F,G), This microfacies also contains fragments of limestone surrounded by spar (Figure 8J).

3.4.10 | Micrite dominating fossiliferous wackestone subfacies

This microfacies is comprised of medium-large deformed foraminifera bioclasts in micritic material. Stylolites and micritisation are frequent in bioclasts.

3.4.11 | Microspar dominating fossiliferous packstone subfacies

This subfacies shows a relatively large grain size. The spar surrounds the limestone clasts, which are scattered in the micritic material. This subfacies is characterised by the presence of large bioclasts and spar (Figure 8K,L). This is a lateral extension of the micrite-dominated fossiliferous wackestone subfacies.

4 | DISCUSSION

4.1 | Interpretation of the Lockhart limestone microfacies

The first microfacies (LMF 1) from the base of the Lockhart Limestone is similar to FZ8 and FZ9 of Flügel and Munnecke (2010). The abundance of lime mud in this microfacies suggests deposition in a low-energy environment with relatively calm, shallow water, most likely on a shallow shelf in an inner ramp setting (Flügel & Munnecke, 2010; Vaziri-Moghaddam et al., 2006). Dolomitic recrystallisation of micrite during diagenesis results in the development of micritic dolomite (Janjuhah et al., 2019; Xi et al., 2015). A wavy laminated subfacies may indicate the influence of fair-weather wave base.

The second microfacies (LMF 2) from the middle section of the formation is the same as the SMF-18 of Flügel and Munnecke (2010) and Wilson (1974). It is interpreted as forming below wave base in calm, shallow water. The presence of Dascycladacean algae, in particular, indicates shallow water depths of 5–15 m in an inner to upper middle ramp (Hanif et al., 2014). These algae are typical of the depositional environment found between the inner and middle shelf areas. Awais et al. (2019) referred to similar facies as 'electrofacies 3' in their studies, describing them as deposits formed within the inner-middle shelf region. The appearance of (green algae) *Gymnocodiacea* and the dominance of benthic foraminifers directed the depositional environment in the photic and oxygenated middle shelf region just below the storm wave base (Abasaghi et al., 2020; Flügel & Munnecke, 2010). This
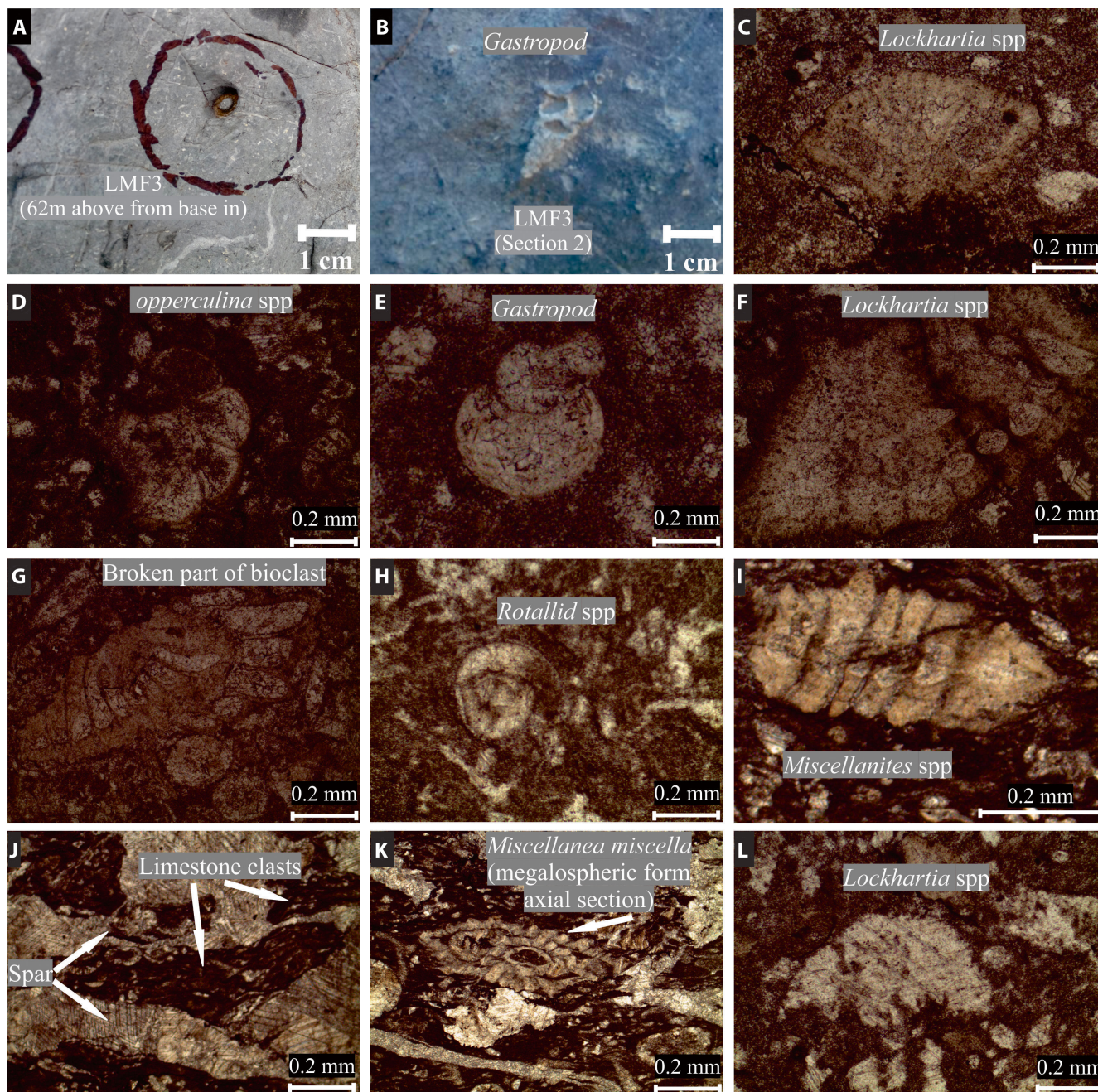
FIGURE 8 Photomicrographs of the benthic foraminiferal wacke–packstone microfacies (LMF 3): (A and B) Exceptional megascopic fossil; (C through L) Bioclasts identified in LMF3.

mudstone–packstone microfacies is dominated by a visible pattern composed of algae, mixed and broken fossils, *Miscellanea miscella* and *Coskinolina* bioclasts.

The third microfacies (LMF 3) from the top section of the Lockhart Limestone has the same fossil composition as Flügel and Munnecke (2010) facies assemblages SMF8 and 9, and Wilson (1974) FZ4, FZ5. The presence of a high micrite concentration indicates deposition in a low-energy environment. Micritisation, cementation and spar are common in a middle shelf environment (Wadood et al., 2021). Deposition on the middle shelf is suggested in conjunction

with the fossil content of these facies. The majority of the fossils found indicate normal salinities during deposition of this microfacies. Gastropods suggest a shallow-marine shelf environment with normal salinity, while the presence of small-sized Milliolid and Nummulites spp. supports relatively high salinities and subtidal depths of 20–130 m with lime mud precipitation (Reiss & Hottinger, 2012). Limestone clasts surrounded by spar represent a high-energy environment. Clasts with similar textures indicate intraclast origins within the formation. The original micrite has recrystallised to form microspar, enclosing the hardened

Diagenetic Processes	Diagenetic Environment		
	Marine	Meteoric	Burial
Micritisation	▬▬▬		
Cementation		▬▬▬▬	
Neomorphism	▬		
Dissolution		▬▬▬▬	
Compaction (Physical and Chemical)			▬▬▬
Fracture and Veins Filling			▬

FIGURE 9 Based on petrographic observations, a proposed diagenetic process for the studied area.

limestone clasts. The wacke–packstone biomass shows a clear pattern of fading algae, Coskinolina, subsequently replaced by *Assilina* spp., as well as variegated species such as *Lockhartia haimei*, *Lockhartia conditi*, *Miscellanites primitivus*, Gastropods, *Operculina* and Miliolids, indicating a shift from orthochem-allochem components from LMF1 to LMF3 microfacies respectively. The presence of *L. haimei* and *Miscellanea miscella* zone fossils in the Lockhart Limestone indicates that it is Thanetian in age (Figure 8K) (Sameeni et al., 2013).

4.2 | Diagenesis

Diagenesis is a process of classical transformation in the rocks from deposition to burial and is most commonly found in carbonate reservoir rocks. However, in the Himalayas, post-depositional diagenesis occurred due to the intense compressional tectonic forces in the region (Bilal et al., 2022). Micritisation, cementation, dissolution, replacement, compaction (both physical and chemical), fracturing and calcite filling are all examples of diagenetic processes that have occurred in the Lockhart Limestone (Figures 5, 7 and 9). These modifications have had significant effects on the pore-throat structure of the rocks. Janjuhah and Alansari (2020) suggest that as these systems adapt to changes in their environment, they change in a unique way. As shown by the petrographic features of the examined samples, diagenetic processes have overprinted the pore size distribution.

The micrite envelope, as seen in Figures 6C,D and 9, is the first diagenetic process to occur in low-energy and slow-sedimentation conditions (Figure 7C,D) (Janjuhah et al., 2021; Morad et al., 2018; Saleem et al., 2020; Tucker & Wright, 2009). Syn-sedimentary micritisation is defined by Brett and Brookfield (1984) as the development of micritic bio-erosion fringes that penetrate deep into the grain. Modification and deposition of micrite envelopes occur simultaneously (Ge et al., 2020; Tomašových et al., 2022).

Moderate to complete grain micritisation occurred in the skeletal components (Figure 7H,I,K). The presence of boring organisms and significant levels of microbial activity have also been reported. The micrite matrix indicates a later stage of micritisation (Figure 7I).

Indications of calcite and dolomite cement have been observed (Figure 6C,D,F through I,K). It has been reported that calcite cement precipitates under marine diagenetic conditions (De Boever et al., 2017; Mueller et al., 2020; Shuster et al., 2018; van Smeerdijk Hood & Wallace, 2012). Foraminiferal skeletons exhibit syntaxial overgrowth cement, which is characterised by a micrite envelope with an incompletely formed outer layer (Figure 8D,E). Mechanical compaction and certain pore-lining cements come after the syntaxial cements (Al Areeq et al., 2016). Syntaxial overgrowths are associated with bioclasts and open-grained sedimentary textures that are replaced by pore fluids precipitations (Alsuwaidi et al., 2021). Calcite cement fills the intraparticle, mouldic and vuggy pores to a far greater extent than any other material.

Carbonate minerals dissolve mostly because of their solubility (Toner & Catling, 2020). The 'dissolution' of metastable bioclasts in meteoric water is referred to in the literature (Budd, 2002; Janjuhah et al., 2017b; Tucker & Wright, 2009). Secondary porosity develops during the early-late phases of porosity development, and it shows a high degree of dissolution in the samples studied (Figures 6E and 9). Seawater or a shallow burial depth might have facilitated the early dissolution of aragonite (Ge et al., 2022). Mouldic and vuggy porosities were formed during the late stages due to the dominance of fabric-to-non-fabric-selective dissolution (Figure 6K,I). Overburdened stresses are the primary source of compaction, but temperature changes (geothermal gradient) may also play a role by increasing pore pressure and leading to changes in pore structure as a result of chemical interactions between water and rock grains (Swarbrick, 2012). Overburden pressure is responsible for the observed grain-to-grain contacts, the observed

distribution pattern of various grains, and the reported fractures (Figure 7B,D). Grain fracture, breaking and close packing are all signs of mechanical compaction.

Fine-grained calcite matrices have subhedral and euhedral calcite crystals that are between 5 and >20 μm in diameter (Ionov & Harmer, 2002). In the Lockhart Limestone, the alteration of high-magnesium calcite (micrite) into low-magnesium calcite (microspar) is a common occurrence, characterised by the formation of isolated patches of microspar (Figure 7F). Many stylolites have been identified in the Lockhart Limestone (Figure 5D). Stylolites are a late stage diagenetic process characterised by irregular seams of insoluble residues of the parent rock and formed when compacted grains continue to dissolve at planar and sutured contacts. Carbonate rock fractures also occur as significant secondary structures as a result of either compaction or as a result of local tectonic activity (McMahon et al., 2017). Additionally, micro-fractures may be caused by extensional movements and natural hydraulic fracturing (Janjuhah et al., 2021; Jin et al., 2021). The filling of the fractures by calcite demonstrates that diagenesis occurred long after the rocks were buried.

4.3 | Depositional environment

The Lockhart Limestone was deposited during the Thanetian transgression of the Ceno-Tethys Ocean (Hanif et al., 2014), which resulted in flooding of the Indian Plate margins (Shah, 2009). The continuous collision of the Indian and Eurasian plates resulted in cyclic movement of the coastline and the formation of sedimentary sequences characterised by limestone and chert deposition (Jade et al., 2017). Microfacies analysis, incorporating information from the fossil content (Figure 4B), indicates that the Lockhart Limestone was deposited on a carbonate shelf that formed in a shallower, inner-middle shelf environment (Figure 10). In the inner-middle shelf of the Ceno-Tethys Ocean, a large group of benthic foraminifera was found to include *Rotaliids*, *Miscellanea*, *Lockhartia*, *Operculina* and *Nummulites* species (Figure 10A through I).

This environment is often observed in shallow shelf to open-marine settings. Access to the open ocean is commonly through a narrow channel or flooding waves. The chert content of the lower Lockhart Limestone varies (LMF 1 and LMF 2). (Table 2). This is produced by the precipitation of silica shelled organisms, which is especially common during periods of falling sea level.

A decrease in mudstone facies and Dascycladacean green algae, along with an increase in benthic foraminifera, indicates a change from an inner shelf to middle shelf environment (Figure 10). Also, both Yates and Bradshaw (2018) and Ameen (2008) stress the importance of the Thanetian succession in the Tethyan realm. However, the Thanetian transgression should not be misinterpreted as a regional sea-level rise. In general, the UIB's hinterland experienced regionally unequal changes in elevation from the late Cretaceous to the early Palaeocene, i.e., during India's collision with Eurasia. The northern part of the basin, for example, the Kohistan Island Arc, was uplifted earlier than the eastern part of the basin's marginal areas (Ullah et al., 2020). This is why the Thanetian transgression has different geographical and temporal effects throughout the UIB. Furthermore, the eastern part of the basin witnessed a down-folding event during the Thanetian owing to an angular motion of the Indian Plate (Jade et al., 2017). This finally resulted in the formation of the HKS on the eastern margin of UIB. Finally, towards the end of the sedimentary sequence, a drop in sea level is visible, corresponding to an uplift in the later Palaeocene emergence. This regression finally resulted in sedimentary conditions common to the overlying strata, which favoured the development of tropical coal and bauxite deposits (Qasim et al., 2020).

4.4 | Sequence stratigraphic analysis

In the case of the Lockhart Limestone, depositional interpretation (or facies analysis) may aid in sequence identification and correlation while also providing knowledge of the sedimentary conditions in the examined location. The Lockhart Limestone originated on a typical carbonate homoclinal shelf, which develops at low slope angles during times of minimal tectonic activity, resulting in relatively uniform deposition over large regions. Transitional deposition occurs below the wave base from the inner (near shoreline) to the middle shelf (deeper) zones (Adams & Diamond, 2019). Following a basin-wide unconformity, facies alternations (together with changes in fossil material) between LMF1, LMF2 and LMF3 (Figures 3 and 4) indicate two very short-term cycles of deepening and shallowing upwards, coinciding with transgression and regression cycles in the area. These short-term cycles might be explained by the continuing Himalayan Orogeny and the associated down-throw subsidence of single tectonic blocks in the region. The sequence boundaries are clearly evident. As they moved from the first (LMF1) to upper microfacies, the targeted strata formed a shelf margin systems tract (SMST) (a sequential basal subdivision) (LMF2, 3). A reverse succession from LMF2 and 3 to LMF1 overlays this system tract, suggesting a highstand systems tract (HST) and pointing to the maximum regression. As a result, the Lockhart Limestone deposition may be classified as a type 3 transgressive–regressive systems
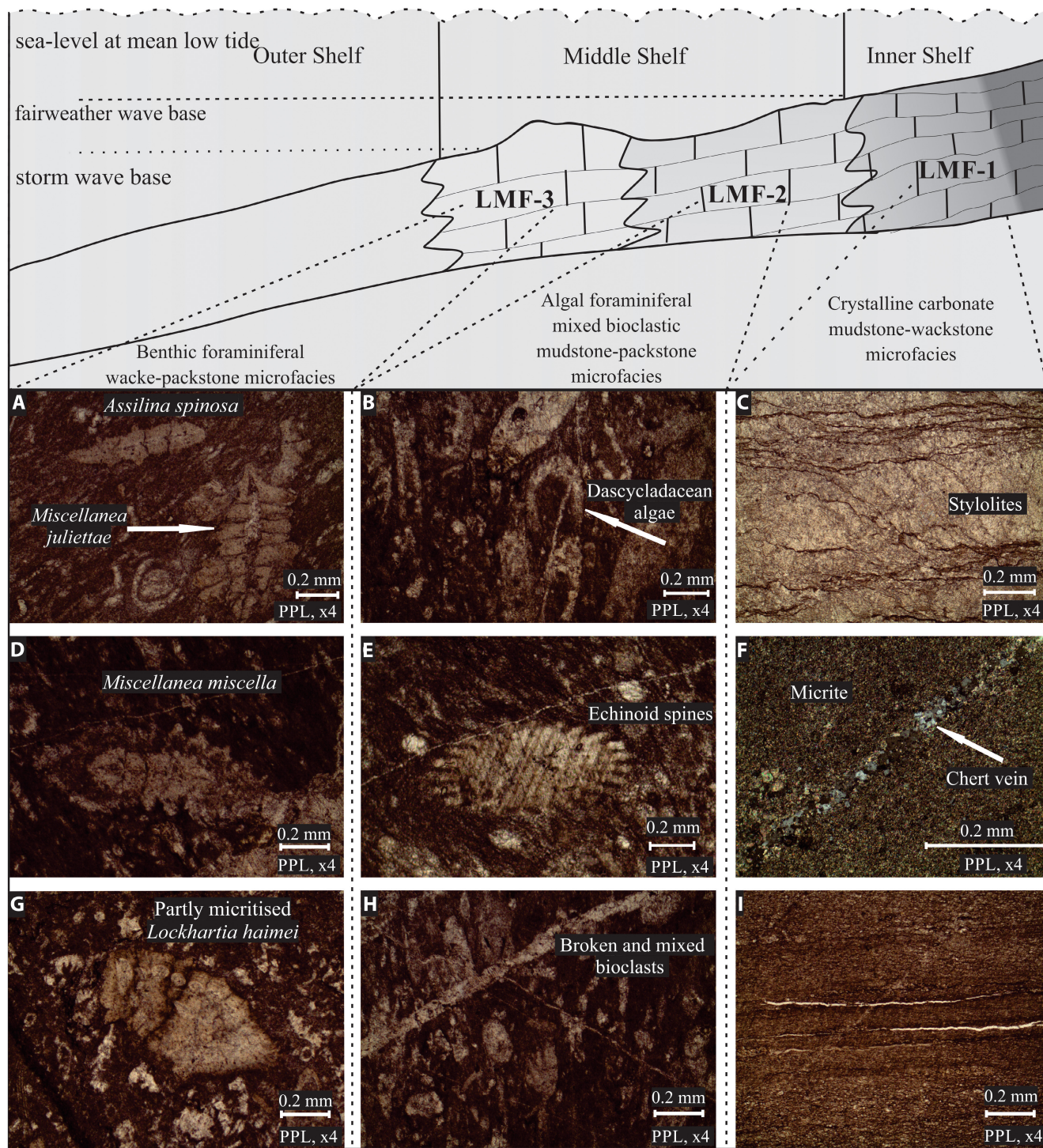
FIGURE 10 Sectional model of inner-outer carbonate shelf and representative deposits.

tract. These cycles are characterised by generally shallow but below-wavebase transgression shelf deposits with a deepening upward sequence, shelf conditions shifting landward, and favourable reservoir features (Kontakiotis et al., 2020; Posamentier, 2002). These reservoirs are generally a few tens of metres thick (Steela et al., 2000). In this case, however, the formation thickness averages 151 m.

4.5 | Regional correlation

Nodular carbonate rocks were deposited on the shallow shelf of the Ceno-Tethys Ocean during the upper Palaeocene. The Lockhart Limestone appears together with the Zongpu Formation and Jahrum Formation, all of which were deposited in the Thanetian period (Awais et al., 2019; Reza, 2014; Yang et al., 2017). These carbonates are known
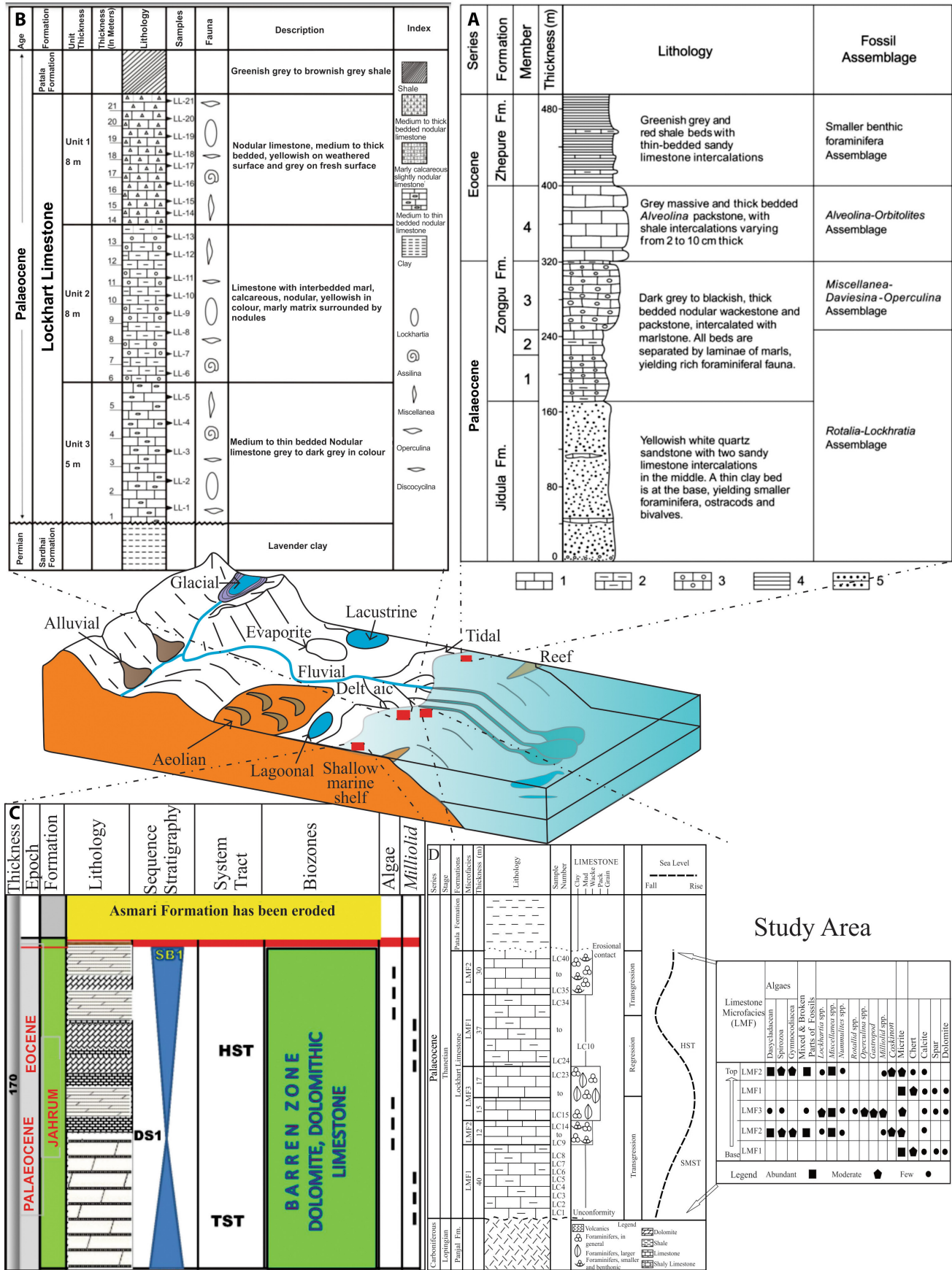
FIGURE 11   Regional depositional model of Upper Palaeocene strata showing lithologs of: (A) Tibet (China), (B) Salt Range (IB, Pakistan), (C) Zagros Basin (Iran) and (D) Study area Eastern margin of UIB (Azad Jammu and Kashmir area) (modified from Awais et al., 2019).

TABLE 3 Regional correlation of Upper Palaeocene rocks. Marine units are shown in blue while, white colour indicate non-marine sequences (modified from Jiang et al. 2016). Colum's are modified from (1) Berggren and Pearson (2005), (2) Jiang et al. (2016), (3) Bilal et al. (2022), (4) Bhatia and Bhargava (2006), (5) Tiwari and Tripathi (1987), (6) Pivnik and Wells (1996), (7) Najman et al. (2008).

Epoch	Age	Larger Benthic Foraminifer zonation 1	Tethys Humalaya Gamba-Tingri 2	Kashmir syntaxis 3 (This Study)	Lesser Himalaya Simla 4	Lesser Himalaya Siang 5	Kohat 6	Bengal Basin 7	Zagros Basin 8
Miocene	Aquitanian	SBZ24			Kasauli Formation	Dafla Formation	Murree Formation		
Oligocene	Chattian	SBZ23		Kuldana Formation	Dagshai Formation			Barail Group	
Oligocene	Chattian	SBZ22b		Kuldana Formation	Dagshai Formation			Barail Group	Asmari Formation
Oligocene	Rupelian	SBZ22a		Kuldana Formation	Dagshai Formation			Barail Group	Asmari Formation
Oligocene	Rupelian	SBZ21		Kuldana Formation	Dagshai Formation			Barail Group	Asmari Formation
Eocene	Priabonian	SBZ20, SBZ19, SBZ18	Zongpubei Formation					Kopili Formation	
Eocene	Bartonian	SBZ17	Zongpubei Formation			Yinkiong Formation	Kohat Formation	Sylhet Formation	
Eocene	Lutetian	SBZ14-16	Zhepure Formation		Subathu Formation	Yinkiong Formation	Kohat Formation	Sylhet Formation	
Eocene	Lutetian	SBZ13	Zhepure Formation		Subathu Formation	Yinkiong Formation	Kohat Formation	Sylhet Formation	
Eocene	Lutetian	SBZ12	Zhepure Formation		Subathu Formation	Yinkiong Formation	Kohat Formation	Sylhet Formation	
Eocene	Ypresian	SBZ11	Zhepure Formation	Patala Formation	Subathu Formation	Rengging Formation	Mami khel Formation	Tura Formation	Jahrum Formation
Eocene	Ypresian	SBZ10	Zhepure Formation	Patala Formation	Subathu Formation	Rengging Formation	Mami khel Formation	Tura Formation	Jahrum Formation
Eocene	Ypresian	SBZ5-9	Zhepure Formation	Patala Formation	Subathu Formation	Rengging Formation	Ghazij Group	Tura Formation	Jahrum Formation
Palaeocene	Thanetian	SBZ4	Zongpu Formation	Lockhart Limestone	Subathu Formation	Rengging Formation	Ghazij Group	Tura Formation	Jahrum Formation
Palaeocene	Selandian	SBZ3	Zongpu Formation	Lockhart Limestone	Subathu Formation		Ghazij Group	Tura Formation	Jahrum Formation
Palaeocene	Selandian	SBZ2	Zongpu Formation	Lockhart Limestone	Subathu Formation		Ghazij Group	Tura Formation	Jahrum Formation
Palaeocene	Danian	SBZ1	Zongpu Formation	Lockhart Limestone	Subathu Formation		Ghazij Group	Tura Formation	Jahrum Formation

as the upper member 3 of the Zongpu Formation in the Tibet region of China (Jiang et al., 2016). Furthermore, the limestone of the Zongpu Formation is nodular, thickly bedded and classified as wackestone or packstone (Figure 11A). Miscellanea and Operculina species were identified as the dominant fossils (Wan et al., 2010). At the same time, the Lockhart Limestone was deposited in the IB's Salt Range (Figure 11B) and Murree areas, with similar nodular habits and medium to large bedded limestone, composed of a wide range of *Miscellanea* spp, *Discocyclina* spp, *Lockhartia* spp, gastropods, *Milliolid* spp, pelecypods, *Operculina* spp and ostracods (Ahmad et al., 2014; Sameeni et al., 2013; Yaseen et al., 2011).

The basin's nodular carbonates serve as excellent reservoirs (Awais et al., 2019; Shakir et al., 2019). Similar rocks have been identified in Iran's Zagros Basin as part of the Jahrum Formation. The fossil assemblage in this formation is comprised of similar biota (Reza, 2014; Figure 11C).

Shallow shelf conditions in the Ceno-Tethys Ocean during the Thanetian Palaeocene resulted in the deposition of the Lockhart Limestone on the eastern margin of UIB (Figure 11D). The Lockhart Limestone under study is comparable to the Zongpu Formation upper member 3 and the Jahrum Formation middle part (Table 3). The limestone in the study area is nodular in habit and contains a diverse range of benthic foraminifers. The examined formation seems to be capable of sustaining a hydrocarbon reservoir in the IB and surrounding parts of the world.

Khattak et al. (2017) studied the Lockhart Limestone near Islamabad (Potwar Basin). That contribution recognised the first microfacies as LH-MF 1 from the end of early transgression (corresponding to LMF3; Figure 3A). In the centre of the section, where a reverse succession is redeposited, the research revealed an identical microfacies to LH-MF 2 with reference to LMF1 above the centre of our study area (LMF1) (Figure 4A). This contribution found

the uppermost (Figure 3A) microfacies (LMF2) equal to the third microfacies (LH-MF 3) of Khattak et al. (2017). This comparison shows that the lower 52 m of the succession is absent in their study area. This may also explain the reduced thickness of the Lockhart Formation on the UIB's eastern margin in Khattak et al. (2017) compared to this study.

Furthermore, not only are equivalent microfacies detected in both places, but so is the same depositional environment, which is referred to in both studies as the inner-middle shelf. This is an important discovery because the similar palaeo-depositional environment demonstrates the extensive reach of a shallow water carbonate shelf in the Thanetian Palaeocene from the Potwar Basin to the eastern margin of the UIB (>100 km), suggesting deposition in a single basin.

5 | CONCLUSIONS

Microfacies analysis and diagenesis studies were conducted (Lockhart limestone) in order to shed light on the composition of the carbonate shelf and reservoirs in Palaeocene strata. On the eastern margin of UIB, the Thanetian age Lockhart Limestone was deposited in a shallow carbonate shelf environment. From base to top, a gradual change from orthochems to allochems has been recorded in these three microfacies (LMF1, LMF2 and LMF3). The Lockhart Limestone and other formations found along the eastern margin of UIB share similar depositional environments, pointing to a single basin of deposition. Deposition of the Lockhart Limestone was accompanied by a type 3 transgressive–regressive systems tract, or fourth-to sixth-order cycles, as well as a SMST and a HST.

Micritisation, dissolution, cementation, fracturing and physical and chemical compaction all played a role in determining the final reservoir characteristics in the Lockhart Limestone. Therefore, in the Palaeocene limestone, stylolite features and fractures have enhanced the reservoir quality. Nodular rocks of Lockhart Limestone are found synchronous with the Zongpu Formation of China and the Jahrum Formation of Iran, which act as excellent reservoirs in their respective areas. A careful examination of microfacies and diagenesis may provide a better basis for selecting reservoir targets in the study region. As a result of the Lockhart Limestone's displaying favourable reservoir characteristics the formation's rocks have the potential to become a significant hydrocarbon reservoir.

CONFLICT OF INTEREST STATEMENT
The authors declare no conflict of interest.

DATA AVAILABILITY STATEMENT
The datasets used in this work are already included within the article. However, a separate file of data is also available on request to the corresponding authors.

ORCID
Ahmer Bilal https://orcid.org/0000-0003-4083-5056
Hammad Tariq Janjuhah https://orcid.org/0000-0002-1522-5988
George Kontakiotis https://orcid.org/0000-0001-9371-6726

REFERENCES
Abasaghi, F., Mahboubi, A., Gharaie, M.H.M. & Khanehbad, M. (2020) Occurrence of Zoophycos in the Ruteh Formation, Middle Permian (Guadalupian), Central Alborz, Iran. *Palaeoenvironmental and Sequence Stratigraphy Implications*, *298*(3), 285–309.

Adams, A. & Diamond, L.W.J. (2019) Facies and Depositional Environments of the Upper Muschelkalk (Schinznach Formation, Middle Triassic) in Northern Switzerland. *Swiss Journal of Geosciences*, *112*(2), 357–381.

Afzal, J., Williams, M. & Aldridge, R.J. (2009) Revised Stratigraphy of the Lower Cenozoic Succession of the Greater Indus Basin in Pakistan. *Journal of Micropalaeontology*, *28*(1), 7–23.

Ahmad, S., Kroon, D., Rigby, S., Hanif, M., Imraz, M., Ahmad, T., Jan, I.U., Ali, A., Zahid, M. & Ali, F. (2014) Integrated paleo-environmental, bio-and sequence-stratigraphic analysis of the Late Thanetian Lockhart limestone in the Nammal Gorge Section, Western Salt Range, Pakistan. *Journal of Himalayan Earth Science*, *47*(1), 1–9.

Akhtar, S., Rahim, Y., Hu, B., Tsang, H., Ibrar, K.M., Ullah, M.F. & Bute, S.I. (2019) Stratigraphy and structure of Dhamtaur Area district Abbottabad, Eastern Hazara, Pakistan. *Open Journal of Geology*, *9*(1), 57.

Al Areeq, N.M., Soliman, M.A., Essa, M.A. & Al-Azazi, N.A. (2016) Diagenesis and Reservoir quality analysis in the Lower Cretaceous Qishn sandstones from Masila oilfields in the Sayun–Masila Basin, Eastern Yemen. *Geological Journal*, *51*(3), 405–420.

Ali, S.K., Janjuhah, H.T., Shahzad, S.M., Kontakiotis, G., Saleem, M.H., Khan, U., Zarkogiannis, S.D., Makri, P. & Antonarakou, A. (2021) Depositional sedimentary facies, stratigraphic control, Paleoecological constraints, and Paleogeographic reconstruction of late Permian Chhidru formation (Western Salt Range, Pakistan). *Journal of Marine Science and Engineering*, *9*(12), 1372.

Alsuwaidi, M., Mohamed, A.A., Mansurbeg, H., Morad, S., Alsuwaidi, A., Al-Shalabi, E.W., Gomes, J., Al-Ramadan, K.,

Mohammed, I.Q. & Farouk, S. (2021) Depositional and diagenetic controls on reservoir quality of microporous Basinal Lime Mudstones (Aptian), United Arab Emirates. *Sedimentary Geology*, *420*, 105925.

Ameen, F.A. (2008) Sequence stratigraphy and Basin modeling of the Eocene succession from Kurdistan Region, Northeastern Iraq. In: *GEO 2008. European Association of Geoscientists & Engineers*. Tulsa, OK: American Association of Petroleum Geologists, pp. cp-246–cp-00065.

Ashraf, M. & Chaudhary, M. (1984) Petrology of Lower Siwalik Rocks of Poonch Area, Kashmir. *Journal of Geology*, *2*, 1–10.

Awais, M., Ullah, F., Khan, N., Ghani, M., Siyar, S.M., Wadood, B. & Mukhtiar, A. (2019) Investigation of reservoir characteristics, depositional setting and T–R sequences of the Lockhart limestone of Meyal Oil Field, Pakistan: A petrophysical approach. *Journal of Petroleum Exploration and Production Technology*, *9*(4), 2511–2530.

Badshah, M., Gnos, E., Jan, M. & Afridi, M. (2000) Stratigraphic and tectonic evolution of the Northwestern Indian Plate and Kabul Block. *Geological Society London Special Publications*, *170*(1), 467–476.

Berggren, W.A. & Pearson, P.N. (2005) A revised tropical to subtropical Paleogene Planktonic Foraminiferal Zonation. *The Journal of Foraminiferal Research*, *35*(4), 279–298.

Bhatia, S. & Bhargava, O. (2006) Biochronological continuity of the Paleogene sediments of the Himalayan Foreland Basin: Paleontological and other evidences. *Journal of Asian Earth Sciences*, *26*(5), 477–487.

Bilal, A. & Khan, M.S. (2017) Petrography and provenance of sandstone and studies of shale of Kuldana formation, Kalamula and Khursheedabad area, Kahuta, Azad Kashmir. *Earth Sciences Malaysia (ESMY)*, *1*(1), 21–31.

Bilal, A., Mughal, M.S., Janjuhah, H.T., Ali, J., Niaz, A., Kontakiotis, G., Antonarakou, A., Usman, M., Hussain, S.A. & Yang, R. (2022) Petrography and provenance of the sub-Himalayan Kuldana formation: implications for tectonic setting and Palaeoclimatic conditions. *Minerals*, *12*(7), 794 https://www.mdpi.com/2075-163X/12/7/794

Brett, C.E. & Brookfield, M.E. (1984) Morphology, faunas and genesis of Ordovician hardgrounds from southern Ontario, Canada. *Palaeogeography, Palaeoclimatology, Palaeoecology*, *46*(4), 233–290.

Budd, D.A. (2002) The relative roles of compaction and Early cementation in the destruction of permeability in carbonate Grainstones: A case study from the Paleogene of West-Central Florida, USA. *Journal of Sedimentary Research*, *72*(1), 116–128.

Choquette, P.W. & Pray, L.C. (1970) Geologic nomenclature and classification of porosity in sedimentary carbonates. *AAPG Bulletin*, *54*(2), 207–250.

Davies, L.M. (1930) The Fossil Fauna of the Samana range and some neighbouring areas, the Palaeocene Foraminifera/by Lm Davies.

De Boever, E., Brasier, A.T., Foubert, A. & Kele, S. (2017) What do we really know about early diagenesis of non-marine carbonates? *Sedimentary Geology*, *361*, 25–51.

Dunham, R.J. (1962) Classification of carbonate rocks according to depositional textures.

Ehsan, M., Gu, H., Ali, A., Akhtar, M.M., Abbasi, S.S., Miraj, M.A.F. & Shah, M. (2021) An integrated approach to evaluate the unconventional hydrocarbon generation potential of the Lower Goru Formation (Cretaceous) in Southern Lower Indus Basin, Pakistan. *Journal of Earth System Science*, *130*(2), 1–16.

Flügel, E. & Munnecke, A. (2010) *Microfacies of carbonate rocks: analysis, interpretation and application*. Berlin, Heidelberg: Springer.

Ge, Y., Lokier, S.W., Hoffmann, R., Pederson, C.L., Neuser, R.D. & Immenhauser, A. (2020) Composite micrite envelopes in the Lagoon of Abu Dhabi and their application for the recognition of ancient firm-to hardgrounds. *Marine Geology*, *423*, 106141.

Ge, Y., Wang, H., Tian, Z., Zheng, D., Yi, L. & Han, H. (2022) Marine aragonite evolution in the oxygen-decreasing interval before the Cenomanian-Turonian Ocean Anoxic Event (Oae2) in the Southeastern Neo-Tethys. *Sedimentary Geology*, *429*, 106078.

Hanif, M., Imraz, M., Ali, F., Haneef, M., Saboor, A., Iqbal, S. & Ahmad, S.J. (2014) The inner ramp facies of the Thanetian Lockhart formation, Western Salt Range, Indus Basin, Pakistan. *Arabian Journal of Geosciences*, *7*(11), 4911–4926.

Ionov, D. & Harmer, R.E. (2002) Trace element distribution in calcite–dolomite carbonatites from Spitskop: inferences for differentiation of carbonatite magmas and the origin of carbonates in mantle xenoliths. *Earth and Planetary Science Letters*, *198*(3–4), 495–510.

Jade, S., Shrungeshwara, T., Kumar, K., Choudhury, P., Dumka, R.K. & Bhu, H.J. (2017) India plate angular velocity and contemporary deformation rates from continuous Gps measurements from 1996 to 2015. *Scientific Report*, *7*(1), 1–16.

Janjuhah, H.T. & Alansari, A. (2020) Offshore carbonate facies characterization and reservoir quality of Miocene rocks in the Southern margin of South China Sea. *Acta Geologica Sinica* English Edition, *94*(5), 1547–1561.

Janjuhah, H.T., Alansari, A. & Santha, P.R. (2019) Interrelationship between facies association, diagenetic alteration and reservoir properties evolution in the Middle Miocene Carbonate build up, Central Luconia, Offshore Sarawak, Malaysia. *Arabian Journal for Science and Engineering*, *44*(1), 341–356.

Janjuhah, H.T., Gamez Vintaned, J.A., Salim, A.M.A., Faye, I., Shah, M.M. & Ghosh, D.P. (2017a) Microfacies and depositional environments of Miocene isolated carbonate platforms from Central Luconia, Offshore Sarawak, Malaysia. *Acta Geologica Sinica-English Edition*, *91*(5), 1778–1796.

Janjuhah, H.T., Kontakiotis, G., Wahid, A., Khan, D.M., Zarkogiannis, S.D. & Antonarakou, A. (2021a) Integrated porosity classification and quantification scheme for enhanced Carbonate reservoir quality: implications from the Miocene Malaysian carbonates. *Journal of Marine Science and Engineering*, *9*(12), 1410.

Janjuhah, H.T., Salim, A.M.A., Ghosh, D.P. & Wahid, A. (2017b) Diagenetic process and their effect on reservoir quality in Miocene Carbonate Reservoir, offshore, Sarawak, Malaysia. In: *ICIPEG 2016*. Berlin, Heidelberg: Springer, pp. 545–558.

Janjuhah, H.T., Sanjuan, J., Alquadah, M. & Salah, M.K. (2021) Biostratigraphy, depositional and diagenetic processes in carbonate rocks form southern Lebanon: impact on porosity and permeability. *Acta Geologica Sinica-English Edition*, *95*(5), 1668–1683.

Jiang, T., Aitchison, J.C. & Wan, X. (2016) The youngest marine deposits preserved in southern Tibet and disappearance of the Tethyan Ocean. *Gondwana Research*, *32*, 64–75.

Jin, Y., Fan, C., Fu, X., Meng, L., Liu, B., Jia, R., Cao, S., Du, R., Li, H. & Tan, J. (2021) Risk analysis of natural hydraulic fracturing

in an overpressured Basin with mud Diapirs: A case study from the Yinggehai Basin, South China Sea. *Journal of Petroleum Science and Engineering*, *196*, 107621.

Khan, M.R., Bilali, S.S., Hameed, F., Rabnawaz, A., Mustafa, S., Azad, N., Basharat, M. & Niaz, A. (2018) Application of gravity and magnetic Methods for the crustal study and delineating associated ores in the Western Limb of Hazara Kashmir Syntaxis, Northwest Himalayas, Pakistan. *Arabian Journal of Geosciences*, *11*(6), 1–13.

Khattak, Z., Khan, M.A., Rahman, Z., Ishfaque, M. & Yasir, M. (2017) Microfacies and diagenetic analysis of Lockhart Limestone, Shah Alla Ditta Area Islamabad, Pakistan. *Pakistan Journal of Geology*, *1*(1), 24–26.

Kontakiotis, G., Moforis, L., Karakitsios, V. & Antonarakou, A. (2020) Sedimentary facies analysis, reservoir characteristics and paleogeography significance of the Early Jurassic to Eocene Carbonates in Epirus (Ionian Zone, Western Greece). *Journal of Marine Science and Engineering*, *8*(9), 706.

McMahon, S., van Smeerdijk Hood, A. & McIlroy, D. (2017) The origin and occurrence of subaqueous sedimentary cracks. *Geological Society, London, Special Publications*, *448*(1), 285–309.

Morad, D., Paganoni, M., Al Harthi, A., Morad, S., Ceriani, A., Mansurbeg, H., Al Suwaidi, A., Al-Aasm, I.S. & Ehrenberg, S.N. (2018) Origin and evolution of microporosity in packstones and grainstones in a lower cretaceous carbonate reservoir, United Arab Emirates. *Geological Society, London, Special Publications*, *435*(1), 47–66.

Mueller, M., Igbokwe, O.A., Walter, B., Pederson, C.L., Riechelmann, S., Richter, D.K., Albert, R., Gerdes, A., Buhl, D. & Neuser, R.D. (2020) Testing the preservation potential of early diagenetic Dolomites as geochemical archives. *Sedimentology*, *67*(2), 849–881.

Mughal, M.S., Zhang, C., Du, D., Zhang, L., Mustafa, S., Hameed, F., Khan, M.R., Zaheer, M. & Blaise, D.J. (2018) Petrography and Provenance of the Early Miocene Murree Formation, Himalayan Foreland Basin, Muzaffarabad, Pakistan. *Journal of Asian Earth Sciences*, *162*, 25–40.

Munir, H., Baig, M.S. & Mirza, K.J. (2006) Upper cretaceous of Hazara and Paleogene biostratigraphy of Azad Kashmir, North-West Himalayas, Pakistan. *Geological Bulletin of the Punjab University*, *40*, 40–41.

Najman, Y., Bickle, M., BouDagher-Fadel, M., Carter, A., Garzanti, E., Paul, M., Wijbrans, J., Willett, E., Oliver, G. & Parrish, R. (2008) The Paleogene record of Himalayan erosion: Bengal Basin, Bangladesh. *Earth and Planetary Science Letters*, *273*(1–2), 1–14.

Nawaz, C.M. & Mn, C. (1980) The volcanic rocks of Poonch District, Azad Kashmir. *Geological Bulletin, University of Peshawar*, *13*, 121–128.

Pivnik, D.A. & Wells, N.A. (1996) The transition from Tethys to the Himalaya as recorded in Northwest Pakistan. *Geological Society of America Bulletin*, *108*(10), 1295–1313.

Posamentier, H.W. (2002) Ancient shelf ridges—a potentially significant component of the transgressive systems tract: case study from offshore Northwest Java. *AAPG Bulletin*, *86*(1), 75–106.

Qasim, M., Ding, L., Khan, M.A., Baral, U., Jadoon, I.A., Umar, M. & Imran, M.J.P. (2020) Provenance of the Hangu formation, lesser Himalaya, Pakistan: insight from the detrital zircon U-Pb dating and spinel. *Geochemistry*, *29*(4), 729–743.

Reiss, Z. & Hottinger, L. (2012) *The Gulf of Aqaba: ecological micropaleontology*. Berlin: Springer-Verlag.

Reza, M.M. (2014) Sequence microbiostratigraphy of Jahrum and Asmari formation in Shiraz Area, Zagros, Fars, Iran. *Open Journal of Geology*, *4*, 93–107.

Saleem, M., Naseem, A.A., Ahmad, W., Yaseen, M. & Khan, T.U. (2020) Microfacies analysis, diagenetic overprints, geochemistry, and reservoir quality of the Jurassic Samanasuk formation at the Kahi Section, Nizampur Basin, NW Himalayas, Pakistan. *Carbonates and Evaporites*, *35*(3), 1–17.

Sameeni, S.J., Haneef, M., Shabbir, F., Ahsan, N. & Ahmad, N.J. (2013) Biostratigraphic studies of Lockhart limestone, Changlagali Area, Nathiagali-Murree Road, Hazara, Northern Pakistan. *Science International (Lahore)*, *25*(3), 543–550.

Shah, S.J.T. (2009) Stratigraphy of Pakistan (Memoirs of the Geological Survey of Pakistan). *The Geological Survey of Pakistan*, *22*, 93–114.

Shakir, U., Amjad, M., Mehmood, M., Hussain, M., Abuzar, M., Ahmad, T., Aftab, F. & Tahir, A.J.T. (2019) Structural delineation and hydrocarbon potential evaluation of Lockhart Limestone in Basal Area, Upper Indus Basin, Pakistan. *Nucleus*, *56*(2), 55–62.

Shuster, A.M., Wallace, M.W., van Smeerdijk Hood, A. & Jiang, G. (2018) The Tonian Beck Spring dolomite: marine Dolomitization in a shallow, Anoxic Sea. *Sedimentary Geology*, *368*, 83–104.

Steela, R., Rasmussenb, H., Eidec, S., Neumanc, B. & Siggerudd, E.J.S.G. (2000) Anatomy of high-sediment supply, transgressive tracts in the Vilomara composite sequence, Sant Llorencë Del Munt, Ebro Basin, NE Spain. *Sedimentary Geology*, *138*, 125–142.

Swarbrick, R. (2012) Review of pore-pressure prediction challenges in high-temperature areas. *The Leading Edge*, *31*(11), 1288–1294.

Tiwari, R. and Tripathi, A. (1987) Palynological zones and their climatic inference in the coal-bearing Gondwana of Peninsular India.

Tomašových, A., Gallmetzer, I., Haselmair, A. & Zuschin, M. (2022) Inferring time averaging and hiatus durations in the stratigraphic record of high-frequency depositional sequences. *Sedimentology*, *69*, 1083–1118.

Toner, J.D. & Catling, D.C. (2020) A carbonate-rich Lake solution to the phosphate problem of the origin of life. *Proceedings of the National Academy of Sciences of the United States of America*, *117*(2), 883–888.

Tucker, M.E. & Wright, V.P. (2009) *Carbonate sedimentology*. Chichester: John Wiley and Sons.

Ullah, Z., Li, J.-W., Robinson, P.T., Wu, W.-W., Khan, A., Dac, N.X. & Adam, M.M.A.J.L. (2020) Mineralogy and geochemistry of peridotites and chromitites in the Jijal complex ophiolite along the Main mantle thrust (Mmt or Indus suture zone), North Pakistan. *Lithos*, *366*, 105566.

van Smeerdijk Hood, A. & Wallace, M.W. (2012) Synsedimentary diagenesis in a Cryogenian reef complex: ubiquitous marine dolomite precipitation. *Sedimentary Geology*, *255*, 56–71.

Vaziri-Moghaddam, H., Kimiagari, M. & Taheri, A. (2006) Depositional environment and sequence stratigraphy of the Oligo-Miocene Asmari Formation in Sw Iran. *Facies*, *52*(1), 41–51.

Wadood, B., Khan, S., Li, H., Wadood, J., Ahmad, S. & Khan, A. (2021) The Middle Permian (Capitanian) carbonate platform evolution and stratigraphic architecture of a Neo-Tethys Rim Basin, Central Pakistan. *Geological Journal*, *56*(8), 4080–4101.

Wan, X., Wang, X. & Jansa, L.F. (2010) Biostratigraphy of a Paleocene–Eocene Foreland Basin boundary in southern Tibet. *Geoscience Frontiers*, *1*(1), 69–79.

Wandrey, C.J., Law, B. and Shah, H.A. (2004) Sembar Goru/Ghazij composite Total petroleum system, Indus and Sulaiman-Kirthar Geologic Provinces, Pakistan and India. US Department of the Interior, US Geological Survey Reston, VA, USA.

Wilson, J.L. (1974) Characteristics of Carbonate-platform margins. *AAPG Bulletin*, *58*(5), 810–824.

Xi, K., Cao, Y., Jahren, J., Zhu, R., Bjørlykke, K., Haile, B.G., Zheng, L. & Hellevang, H. (2015) Diagenesis and reservoir quality of the Lower Cretaceous Quantou Formation tight sandstones in the Southern Songliao Basin, China. *Sedimentary Geology*, *330*, 90–107.

Yang, L., Shenghe, W., Jiagen, H. & Jianmin, L. (2017) Progress and prospects of reservoir development geology. *Petroleum Exploration and Development*, *44*(4), 603–614.

Yaseen, A., Rajpar, A.R., Munir, M. & Roohi, G. (2011) Micropaleontology of Lockhart limestone (Paleocene), Nilawahan Gorge, Central Salt Range, Pakistan. *Journal of Himalayan Earth Sciences*, *44*(2), 9–16.

Yates, K.L. & Bradshaw, C.J. (2018) *Offshore energy and marine spatial planning*. Abingdon: Routledge.